Coherence depression in stochastic excitable systems with two-frequency forcing

Na Yu and André Longtin

Citation: Chaos **21**, 047507 (2011); doi: 10.1063/1.3657920
View online: http://dx.doi.org/10.1063/1.3657920
View Table of Contents: http://chaos.aip.org/resource/1/CHAOEH/v21/i4
Published by the American Institute of Physics.

Coherence depression in stochastic excitable systems with two-frequency forcing

Na Yu[1,a)] and André Longtin[2,b)]
[1]*Department of Physics, University of Ottawa, Ottawa, Ontario K1N 6N5, Canada*
[2]*Department of Physics and Department of Cellular and Molecular Medicine, University of Ottawa, Ottawa, Ontario K1N 6N5, Canada*

(Received 30 August 2011; accepted 14 October 2011; published online 29 December 2011)

We study the response of two generic neuron models, the leaky integrate-and-fire (LIF) model and the leaky integrate-and-fire model with dynamic threshold (LIFDT) (i.e., with memory) to a stimulus consisting of two sinusoidal drives with incommensurate frequency, an amplitude modulation ("envelope") noise and a relatively weak additive noise. Spectral and coherence analysis of responses to such naturalistic stimuli reveals how the LIFDT model exhibits better correlation between modulation and spike train even in the presence of both noises. However, a resonance-induced synchrony, occurring when the beat frequency between the sinusoids is close to the intrinsic neuronal firing rate, decreases the coherence in the dynamic threshold case. Under suprathreshold conditions, the modulation noise simultaneously decreases the linear spectral coherence between the spikes and the whole stimulus, as well as between spikes and the stimulus envelope. Our study shows that the coefficient of variation of the envelope fluctuations is positively correlated with the degree of coherence depression. As the coherence function quantifies the linear information transmission, our findings indicate that under certain conditions, a transmission loss results when an excitable system with adaptive properties encodes a beat with frequency in the vicinity of its mean firing rate. [doi:10.1063/1.3657920]

The spectral coherence function, used in a wide variety of biological and engineering studies, measures the linear correlation between input and output as a function of frequency. In this paper, we studied the coding of neuron models to signals made up of the sum of two sinusoidal waveforms with arbitrary (but relatively close) frequencies, as well as noise on one of the frequency components; this latter noise is meant to represent random motion of a stimulus source and other environmental fluctuations. This is a generic signal in electrosensory systems, and in other senses such as the auditory sense. We looked at coherence between the raw signal, as well as its envelope (i.e., amplitude modulation) and the output spike trains of the neuron models. We found that a neuron model with a dynamic firing threshold—a well-known form of adaptive dynamics—can improve the coherence in the presence of amplitude modulation noise and additive noise. However, the coherence is depressed by noise when the beat frequency (the difference on frequencies of two sine functions) overlaps the intrinsic neuronal firing rate. Through spectral analysis, we observed a strong frequency synchrony between envelope cycles and spike events caused by resonance when the beat frequency is near the intrinsic firing rate. This synchrony diminishes the role of dynamic firing threshold in regulating the instantaneous firing rate. Hence, amplitude modulation noise suppresses envelope—spike train coherence by causing variability in both envelop waveforms and spike timing. A larger noise intensity leads to a higher depression level. This coherence depression is relevant in the context of socially interacting weakly electric fish, but also for the response of the ear to multiple sounds.

I. INTRODUCTION

The effects of noise on excitable are numerous and have received wide attention in the last decades.[1] A common problem has been the reliable detection and transmission of time-varying stimuli. For a subthreshold (i.e., weak) signal, the well-known stochastic resonance effect (SR) states that a single threshold system acquires an enhanced detectability to this signal when noise is at an appropriate intensity.[2,3] This has also been studied for noisy signals via linear correlation measures.[4,5] For a suprathreshold stochastic signal, the integration of a network with N independent noisy devices can maximize the amount of information transmitted via suprathreshold stochastic resonance (SSR).[6,7] In the context of electrosensation, stimulation by a common external noise signal has been shown to maximally synchronize an array of non-identical non-coupled noisy neuronal oscillators at a certain intensity of the external noise.[8]

Apart from these and other investigations focusing on single-tone stimuli with noise, there are a few studies where the driving signal consists of two or more frequencies.[9–11] For example, for a mixture of sinusoidal waves with frequencies corresponding to harmonic components of a fundamental frequency, the output shows "ghost" stochastic resonance

[a)]Electronic mail: na.yu@uottawa.ca.
[b)]Electronic mail: alongtin@uottawa.ca.

(GSR) at this fundamental frequency even when absent in the input signal.[9] Two-tone mixtures are also important in auditory research, e.g. in synchrony suppression,[12] as well as in electric circuits, e.g., in synchronization of Schmitt triggers.[13] There is still much to be uncovered and understood when multiple sinusoids of incommensurate frequencies and noise together drive an excitable system.

Here, we will consider a simple case, the superposition of two non-harmonic sine waves with noise on one of the amplitudes. The sine waves can simulate the natural stimuli that a weakly electric fish experiences in the presence of another fish.[14,15] It is also a model for multiple sound waves interfering at the ear, and for musical dyads.[16,17] Of course, systems forced with two sine waves have received a lot of attention in the context of the quasi-periodic route to chaos in the general nonlinear dynamics literature (see e.g., Ref. 18). It is also important in technical applications such as radar and sonar.[19,20]

Such multi-component stimuli are also important in biology because they have fundamental components as well as envelopes that are not present in the fundamental Fourier decomposition of the signal. For example, beats arise, which can be represented by the neural system via nonlinear effects. Envelope processing has been shown to be important in speech reception for human being,[17,21] sound localization[22] and acoustic communication in animals,[23] detection of conspecifics in weakly electric fish,[24] and in the visual system as well.[25–27] However, there is little information on the dynamics of noisy excitable systems in the presence of such stimuli.

Here, the quality of signal transmission in systems forced with two waves will be characterized in terms of the coherence function that has been used in theoretical and experimental studies as a frequency-resolved correlation between input and output.[18,24] We will show, through the numerical comparison between a classical leaky integrate-and-fire (LIF) model and LIF model with dynamic firing threshold (LIFDT), which the introduction of a dynamic threshold improves the detectability of the envelope associated with two sine waves by model neurons in the presence of both amplitude modulation (AM) noise and additive noise, while the envelope - spike train coherence is suppressed when the beat frequency overlaps the intrinsic neuronal firing rate.

Different from the fixed firing threshold in LIF model, the time-dependent threshold of LIFDT model is increased after a spike is generated to mimic refractory properties of the neuron. This introduces intrinsic correlations between interspike intervals (ISIs). The LIFDT model has been used to simulate neurons in sensory systems, for instance electroreceptors of weakly electric fish,[15] pyramidal cells in the cat visual cortex,[28] and cochlear nerve fibres.[29] The dynamic threshold brings a new time scale to the dynamics, and causes resonance effects. It is less clear what its effects are on other direct and intermodulation spectral components. Such spectral profiles have been demonstrated in other experimental and simulation work, including motor units of pericranial muscles,[30] the abducens nerve during eye fixations,[31] and even in heterogeneous networks of inhibitory neurons.[32] We will see how different spectral measures change with noise for the LIFDT model, and lead to certain enhancements and depressions of coherence compared with the standard LIF model.

In the context of electroreception, a prime motivation for our paper, the electroreceptors on the skin of the fish sense the electric organ discharges (EODs) generated by its own or by other nearby fish.[14] The EOD is a highly periodic quasi-sinusoidal wave and each fish has its own signature frequency ranging from 650 Hz to 1100 Hz. Electric fish recognize other fish through the beating of their EODs. These beat frequencies ($\Delta f =$ the difference between any two EOD frequencies) are reflected in the envelope and encoded by the electroreceptors. The generic situation is the one where one of the two sine wave amplitudes fluctuates in amplitude—corresponding to another fish's movement and environmental noise. The implications for electroreceptor dynamics are thus of interest here.

The paper is organized as follows. First, we introduce in Sec. II the neuronal models, the stimulation signal and its envelope, and the coherence function. In Sec. III, we characterize the firing rate characteristics, the spectral profiles of the spike trains, and the coherence between the envelope and the spike train for both models. This allows us to evaluate the impacts of the dynamic threshold, envelope and envelope noise on coherence depression. A sinusoidal amplitude modulation (SAM) is used to further explain the origin of the coherence depression. The paper ends with a discussion and outlook in Sec. IV.

II. MODEL AND MEASUREMENT

A. Stimulus and its modulation envelope

The stimulus considered here is mathematically described as

$$I_{stim} = A_1 \sin(2\pi f_1 t) + (A_2 + \sigma\eta(t)) \sin(2\pi f_2 t) + I + \epsilon\xi(t). \tag{1}$$

Without loss of generality, we take a constant amplitude $A_1 = 1$ mA for the first sinusoidal signal. The second amplitude is stochastic with mean A_2, i.e., $A_2 + \sigma\eta(t)$, where $\eta(t)$ accounts for fluctuations caused by motion or orientation cues.[19,20,33] For electrosensation, it is natural to choose $A_2 \leq A_1$. The f_i are generically incommensurate frequencies less than an octave apart. The constant I represents the bias current set by the complement of ionic channels in the cell. For $A_1 = A_2 = \sigma = \epsilon = 0$, the bias current $I = 0.09$ mA (or 0.4 mA) is the threshold for the LIFDT (resp. LIF) model. We take $I = 0.25$ mA, which corresponds to a suprathreshold signal I_{stim} for both models; in fact I_{stim} can reach maximal value of $I + A_1 + A_2$ periodically without noise. The noise term $\xi(t)$, which is Gaussian white noise with mean zero and unit variance, represents the fluctuation on the synaptic input with standard deviation (STD) ϵ. We also choose $\epsilon \ll \sigma$ so the results will not be affected significantly by this additive noise. The additive noise is nevertheless necessary to obtain the stochastic phase locked behaviour seen in electroreceptors in the presence of A_1 only.[15]

A simple form for the amplitude modulation noise $\eta(t)$ is the Ornstein-Uhlenbeck (OU) process, evolving according

to $\gamma\frac{d\eta}{dt} = -\eta + \sqrt{2\gamma}\zeta(t)$ where $\zeta(t)$ is another Gaussian white noise (independent from $\xi(t)$) with mean zero and unit variance; the correlation time $\gamma = 1$ s. The OU process $\eta(t)$ has mean zero and unit variance, therefore the stochastic amplitude has mean A_2 and STD σ. We also note that the OU process $\eta(t)$, as filtered white noise, evolves on a time scale much slower than f_1, f_2 and $\Delta f \equiv |f_1 - f_2|$. $f_1 = 750$ Hz, $f_2 = 920$ Hz or 945 Hz, $A_2 = 0.2$ mV, $\sigma = 0.2$ mA and $\epsilon = 0.0001$ mA were taken as parameter values for I_{stim} unless otherwise stated.

The envelope of the stimulus I_{stim}, denoted as $E(t)$, is extracted using the Hilbert transform (HT) to produce an estimate of AM. $E(t)$ is defined by

$$E(t) = \sqrt{I_{stim}^2 + \hat{I}_{stim}^2} \tag{2}$$

where $\hat{I}_{stim}$ is the HT of I_{stim}. Reference 34 provides a derivation for the envelope of such multi-component signals similar to I_{stim}. This envelope oscillates according to beat frequency (Δf), but OU process with slow time scale affects its amplitude.

B. LIF Model

The classic LIF model has a fixed firing threshold. This one-variable model is written as

$$\tau_v \dot{v} = -v + rI_{stim}, \tag{3}$$

$$\text{if } v \geq \theta_c, \text{ then } v = 0. \tag{4}$$

where v is the membrane voltage and θ_c is the firing threshold. τ_v determines the exponential decay rate of v, and r is the leak resistance (reciprocal of the leak conductance). According to the threshold condition in Eq. (4), v discharges a spike when $v \geq \theta_c$; and after firing, the membrane potential is reset to zero, as shown in Fig. 1. The parameters are the same as for the LIFDT model below, except that $\theta_c = 0.132$, which is approximately the average of the dynamic threshold θ in the LIFDT model for the parameters of interest. The spike times t_k ($k = 1,2\ldots$) are recorded from numerical simulations, and the spike train can be written as

$$R(t) = \sum_k \delta(t - t_k). \tag{5}$$

C. LIFDT Model

The LIFDT model (see Ref. 15 and references therein) builds on the LIF model by adding an extra differential equation for the threshold:

$$\tau_v \dot{v} = -v + rI_{stim}, \tag{6}$$

$$\tau_\theta \dot{\theta} = \theta_0 - \theta, \tag{7}$$

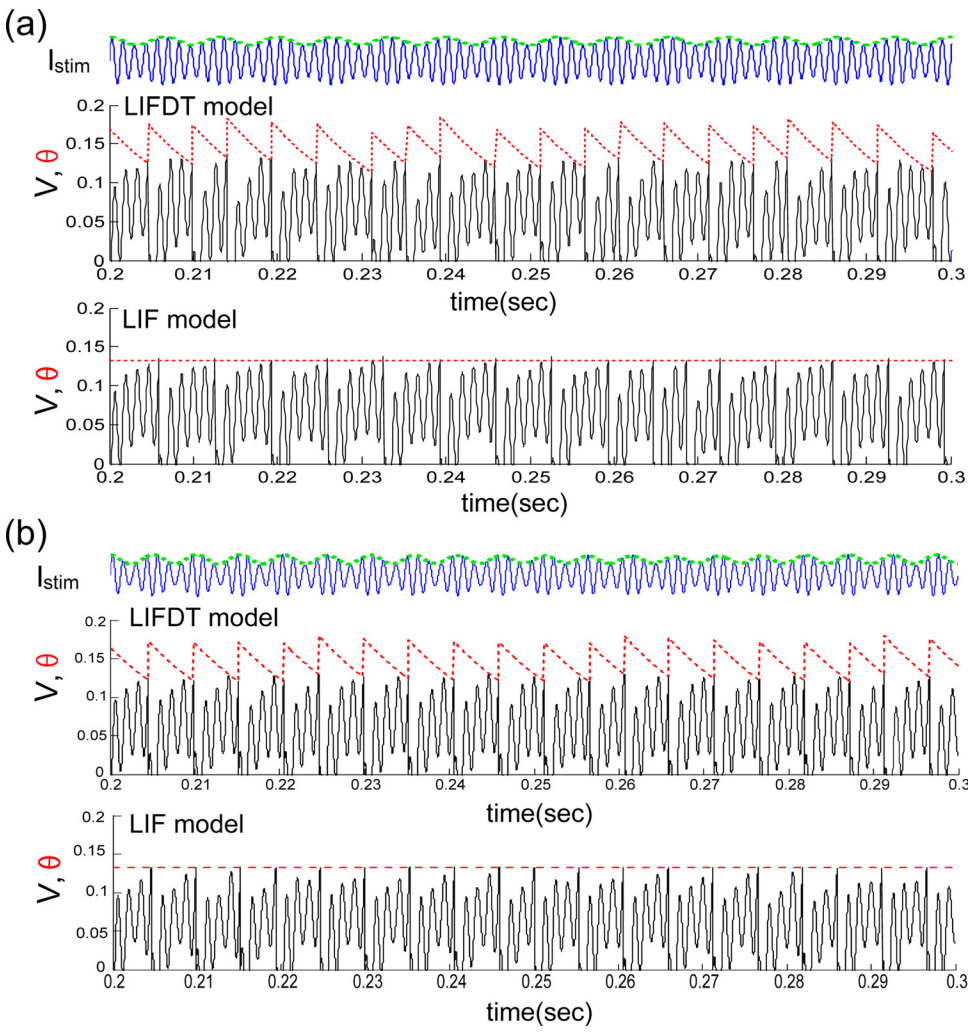

FIG. 1. (Color online) Time series of the LIFDT as expressed in Eqs. (6)-(8) and the LIF model in Eqs. (3) and (4). In response to a same I_{stim} (solid blue lines) with its envelope (dashed green lines), the membrane potential v (solid black), and threshold θ (dashed red) evolve. The models produce a spike every time v touches θ. $f_2 = 920$ Hz and 945 Hz were used for (a) and (b), respectively. Other parameters are $f_1 = 750$ Hz, $A_2 = 0.2$ mA, $\sigma = 0.2$ mA and $\epsilon = 0.0001$ mA, $\tau_v = 1/f_1$ sec, $\tau_\theta = 9/f_1$, $\Delta\theta = 0.05$, $\theta_0 = 0.03$, $I = 0.25$ mA, and r = 0.328 m Ω.

$$\text{if } v \geq \theta, \text{ then } v = 0 \text{ and } \theta = \theta + \Delta\theta. \tag{8}$$

where v is the membrane potential of the neuron, θ is the dynamic threshold, and τ_θ determines the exponential decay rate of θ. Firing occurs (8) whenever v reaches θ. As Fig. 1 shows, following a spike v is reset to zero and θ is updated by $\Delta\theta$. The parameter values are $\tau_v = 1/f_1$ sec, $\tau_\theta = 9/f_1$, $\Delta\theta = 0.05$, $\theta_0 = 0.03$, and $r = 0.328$ mΩ.

D. Coherence function

The coherence function (termed "coherence" below) is used to quantify the linearity of the relationship between the input and the spike train as a function of frequency. It provides an estimate of the lower bound on the mutual information between the input and the output for Gaussian signals.[35,36] For two signals, $X(t)$ and $Y(t)$, it is defined as

$$C_{XY}(f) = \frac{|P_{XY}(f)|^2}{P_X(f)P_Y(f)} \tag{9}$$

where $P_X(f)$, $P_Y(f)$ are, respectively, the auto-spectral densities of $X(t)$ and $Y(t)$, and $P_{XY}(f)$ is the cross-spectral density of $X(t)$ and $Y(t)$. The coherence ranges between 0 and 1, spanning the range from no linear correlation to perfect linear correlation. The cross-spectral densities are also known as frequency dependent gains. The coherence goes beyond those gains by normalizing by the power at the signal and output frequencies, and thus is a signal-to-noise ratio.

The numerical simulations were performed in MATLAB (The MathWorks, Inc., Natick, MA, USA) using a standard Euler-Maruyama integration technique with timestep $= 2 \times 10^{-5}$ s. The mean firing rate, power spectra or coherence functions in Figs. 3-10 were averaged using 50 independent realizations of η and ξ in I_{stim}, and 30 independent ξ were used in Fig. 2(b).

III. RESULTS

We first consider the case where a weakly electric fish consistently emits and senses its own EOD. In this case, $A_2 = \sigma = 0$ in I_{stim}; the resulting mean rate at which a given electroreceptor fires in response to the EOD is known as the intrinsic frequency. For the chosen parameters, these are 167 and 195 Hz for, respectively, the LIF and LIFDT models. As we will see, with the introduction of the second drive at f_2, the mean firing frequency of the LIF model varies significantly from its intrinsic frequency, but that of the LIFDT model changes only slightly.

A. F-I curve and mean firing rate

To understand the processing of signals by these neuron models, it is first necessary to discuss the firing frequency as a function of constant input current (i.e., the F-I curve) for each model, as well as input and output spectral properties. The spectral characteristics of the input and of its envelope are shown in Fig. 2(a). The two sinusoidal frequency components

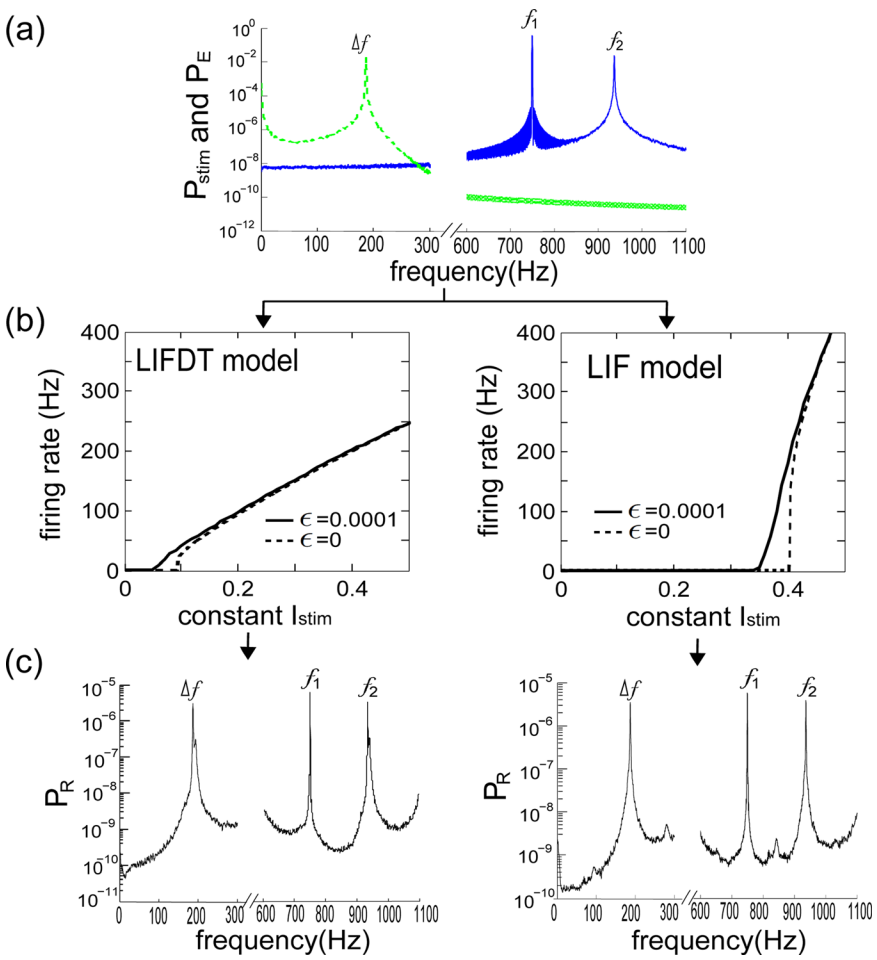

FIG. 2. (Color online) (a) PSDs of the input signal, $P_{stim}(f)$ (solid blue), and of its envelope, $P_E(f)$ (dashed green). (b) F-I curves of LIFDT and LIF models in response to a constant I_{stim} (i.e., $A_1 = A_2 = \sigma = 0$ in Eq. (1)), without additive noise, $\epsilon = 0.0001$ (dashed lines) and with noise using $\epsilon = 0.0001$ (solid lines). The additive noise $\varepsilon\xi$ in Eq. (1) linearizes the threshold nonlinearity of the F-I curves. Thirty independent realizations of ξ were used when $\varepsilon > 0$. (c) PSD of the spike train $R(t)$, $P_R(f)$, has the characteristic frequencies of I_{stim} and its envelope (i.e., f_1, f_2 and $\Delta f = |f_1 - f_2|$). The same parameters as in Fig. 1(b) are used here and in following figures unless stated otherwise.

are clearly present in the raw signal, but not the beat frequency. However, a nonlinear operation, here performed by the envelope extraction (HT),[9,37] reveals the beat frequency.

Figure 2(b) shows the F-I curve for each model, i.e., the mean firing rate, f_m, in response to a constant I_{stim} ($A_1 = A_2 = \sigma = 0$ in Eq. (1)). This curve is a static characteristic of the model because it is computed for constant inputs. It is nevertheless useful to understand how slowly varying inputs are mapped to slowly varying firing rate fluctuations. The noise term $\varepsilon\xi(t)$ in Eq. (1) also linearizes the F-I curves below and near the threshold (see Refs. 38 and 39 and references therein). The addition of the dynamic threshold θ causes a divisive effect on F-I curve,[40] i.e., a decrease in slope of the F-I curve. This implies that a time-varying envelope, caused e.g., by the AM noise $\sigma\eta$, will produce larger firing rate fluctuations for the LIF model compared with the LIFDT model. In other words, the dynamic threshold can diminish the effect of envelope noise; however, at the same time it reduces the dynamic range for coding any relevant envelope fluctuations. We will see this point clearly below in Fig. 3 and the analysis of the spectral peak corresponding to the mean firing rate.

The parameters here are such that spikes occur mostly during the upstrokes of the envelope. The firing rate is in a lower frequency range than f_1 and f_2 in I_{stim}, being rather in the range of the mean frequency of the envelope $\Delta f = |f_1 - f_2|$. The threshold nonlinearity is responsible for this "extraction" of the envelope. This envelope thus has a spectral signature as in Fig. 2(c), which shows the power spectral densities (PSDs) of I_{stim}, $E(t)$ and $R(t)$, denoted by P_{stim}, P_E, and P_R, respectively. One can now think of the beat frequency also as a driving signal. Also, it is known that the LIF models with noise can linearly encode sinusoidal driving forces (see e.g., the theory in Ref. 41), and therefore this model can encode Δf as well as the high frequencies f_1 and f_2 (Fig. 2(c)). The same holds true for the LIFDT, although linear response theory for this model has not yet been developed.

The mean firing rate of the LIF model keeps increasing with its "driving" beat frequency, Δf, basically with a slope of 1 as shown in Fig. 3(a). This implies a good frequency synchronization between $E(t)$ and $R(t)$ for the LIF model for these parameters. However, the firing mechanism of LIFDT model is mediated not only by the driving force but also the dynamic firing threshold θ. This results in ISIs being more restrained near the intrinsic period (i.e., the inverse of intrinsic frequency). Consequently, over the same range of Δf values investigated [150, 250] Hz, f_m is less perturbed away from its intrinsic frequency of 195 Hz than it is in the LIF model.

However, a strong variation of f_m occurs roughly in the range [185, 208] Hz, i.e., in the proximity of the intrinsic frequency, as demonstrated in Fig. 3(b). Over this range, $f_m \approx \Delta f$, indicating strong frequency synchronization induced by resonance. The synchronization suggests a decreased stabilizing role of the dynamic threshold θ, and the LIFDT model behaves more like the LIF model. For example, almost the same firing patterns are seen for both models as shown in Fig. 1(b). We can then further expect that AM noise $\sigma\eta$ has more influence on the firing mechanism of the LIFDT model over this resonant frequency range than elsewhere.

B. Spectral profiles of LIFDT and LIF models

As stated in the Introduction, P_R obtained from the LIFDT model displays distinct peaks at f_m and $f_1 + f_m$ (see Fig. 4(a)). The height and width of these peaks is determined by the coefficient of variation (CV) of ISIs, which is the ratio of standard deviation to the mean of the ISI density. The more regular the ISIs are, the lower the CV, and the higher and sharper these peaks are. AM noise $\sigma\eta$ decreases the height and broadens the peaks at $f_m = 194$ Hz and $f_1 + f_m = 944$ Hz (solid blue line). In contrast, envelope power is strengthened by noise (see Appendix for a more detailed analysis), with an increment of $P_R(f)$ at $\Delta f = 170$ Hz from 4.36×10^{-6} to 6.3×10^{-6} (Fig. 4(a)—although this is difficult to resolve visually on the scale shown.)

By increasing f_2, the spectral peak associated with Δf moves to the right and approaches the peak at f_m. When $f_2 = 945$ Hz and $\Delta f = 195$ Hz (see Fig. 4(b)), these two peaks

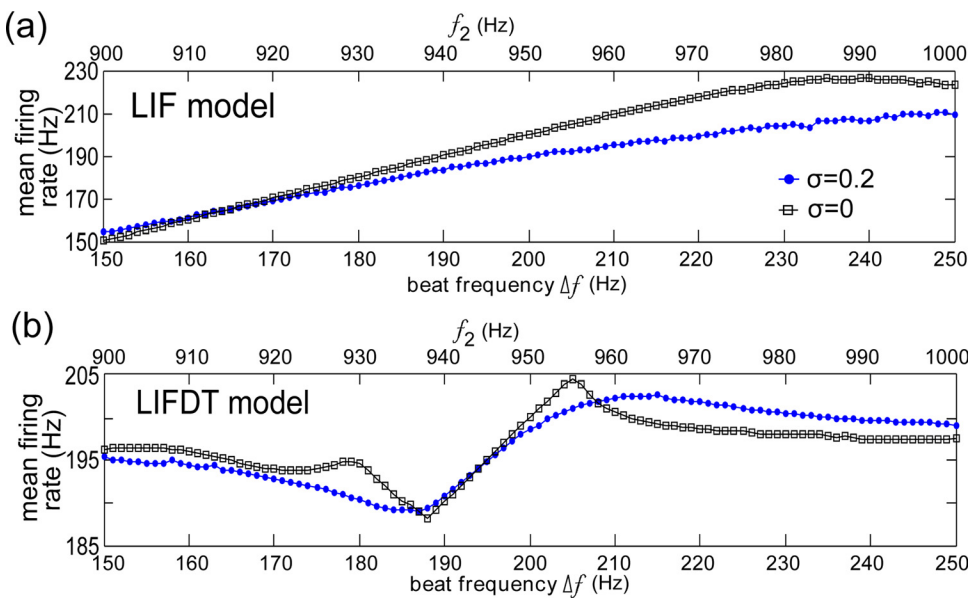

FIG. 3. (Color online) Mean firing rate, f_m, of (a) LIF or (b) LIFDT model as a function of beat frequency Δf (or equivalently f_2 for a fixed f_1) with envelope noise intensities $\sigma = 0$ (black squares) and $\sigma = 0.2$ (blue dots). Fifty independent realizations of η and ξ in I_{stim} were used to average the mean firing rate when $\sigma > 0$.

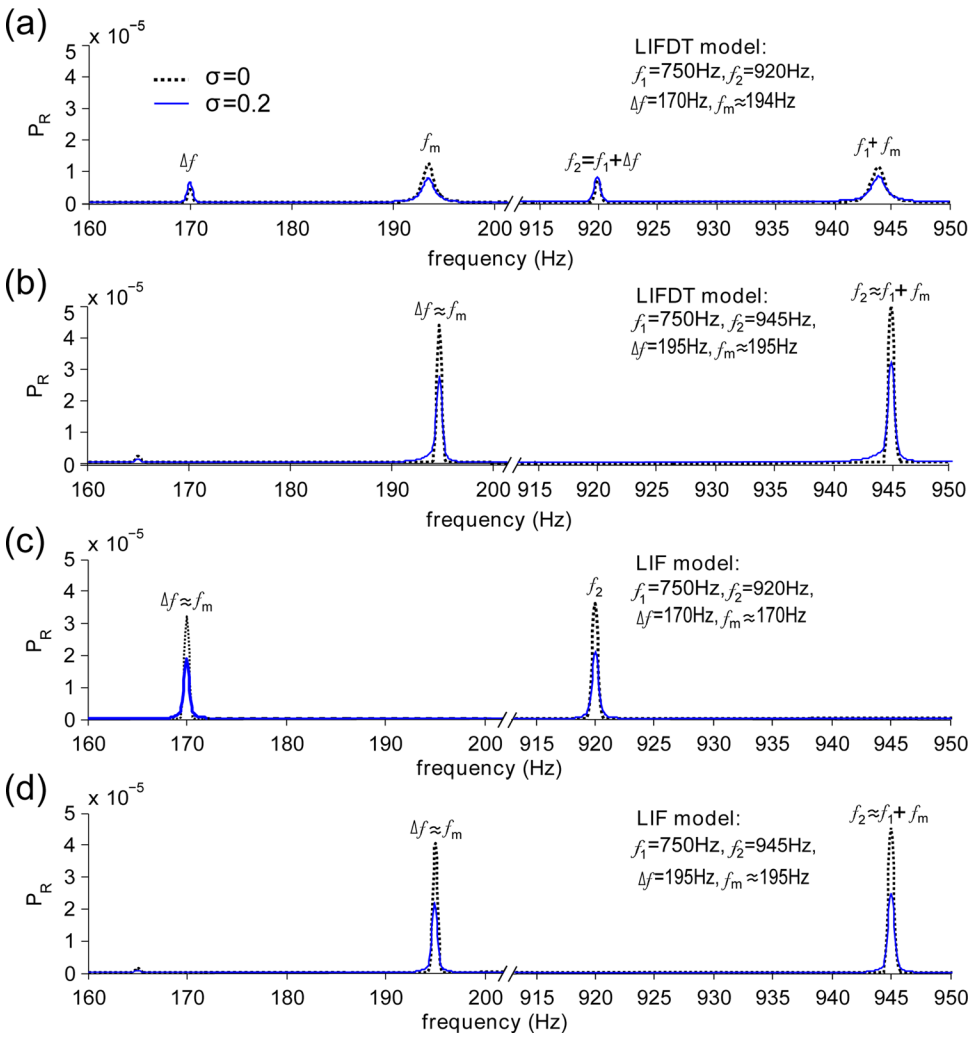

FIG. 4. (Color online) $P_R(f)$ obtained from (a) and (b) LIFDT or (c) and (d) LIF model shows multiple peaks at frequencies marked in the legend. As in Fig. 1, two sets of (f_1, f_2) were used: (750, 920) Hz and (750, 945) Hz. For the LIFDT model, increasing f_2 shifts PSD peak at Δf to the right; the value of $P_R(f_m)$ drops when σ increases from zero (dashed black lines) to 0.2 (solid blue lines). Fifty independent realizations of η and ξ in I_{stim} were used to average the power spectra when $\sigma > 0$.

coalesce and the height reaches a maximum owing to the effect of resonance. However, the spectral peaks of the LIF model at Δf and f_m are overlapped consistently because $f_m \approx \Delta f$ as previously stated (Fig. 3(a)). This also confirms again, from the point of view of spectral profiles, that LIF and LIFDT models share almost identical firing patterns when Δf is in proximity to intrinsic frequency. Envelope fluctuations $\sigma\eta$ seem to decrease P_R at $\Delta f = 195$ Hz further (from 4.2×10^{-5} to 2.6×10^{-5}) in Fig. 4(b). This reduction at $P_R(\Delta f)$ could be interpreted physiologically as the decrease in information coding regarding the envelope.

C. Depression of Envelope-Response Coherence

The coherence function between $E(t)$ and $R(t)$, denoted as C_{ER}, was computed according to Eq. (9) and plotted in Fig. 5. C_{ER} exhibits a peak at Δf. In the absence of AM noise (i.e., $\sigma = 0$), $C_{ER}(\Delta f) \approx 1$ for both models. When noise is present (e.g., $\sigma = 0.2$), the LIF model shows $C_{ER}(\Delta f)$ drops to approximately 0.88 at the beat frequencies. We will see below in Fig. 7 that in fact it drops to [0.85, 0.93] over the whole range of beat frequencies investigated. Interestingly, the LIFDT model has $C_{ER}(\Delta f) = 0.94$ when $\Delta f = 170$ Hz $\neq f_m$ but $C_{ER}(\Delta f) = 0.84$ when $\Delta f = f_m = 195$ Hz. At the same time as this drop in coherence, the coherence peaks are broadened by the noise η.

Similarly, we then computed the values of $P_E(f)$, $P_R(f)$, the cross-PSD between $E(t)$ and $R(t)$ (denoted by P_{ER}), and $C_{ER}(f)$ for the LIFDT model for various Δf. By picking their values at Δf, we could plot the above PSDs as a function of Δf in Fig. 6. P_E is independent of Δf; $P_R(\Delta f)$ and $P_{ER}(\Delta f)$ display bumps over [185, 208] Hz because of the resonance seen in Fig. 4. AM noise $\sigma\eta$ suppresses $P_R(\Delta f)$ and $P_{ER}(\Delta f)$ over this sensitive range while it slightly enhances their values elsewhere. This noise also induces the coherence depression over this sensitive regime, with $C_{ER}(\Delta f)$ reaching a minimum at the intrinsic frequency of 195 Hz.

In order to quantify the influence of AM noise on each function and explain the coherence depression, we calculated the ratio of specific function values in the case of $\sigma = 0.2$, denoted as $F(\Delta f, \sigma = 0.2)$, to those function values in the case of $\sigma = 0$, denoted as $F(\Delta f, \sigma = 0)$. This was done for $F = P_E$, P_R and $|P_{ER}|^2$, i.e., the blue dots divided by black squares in Figs. 6(a)-6(c). The ratio for P_E, marked as pink stars in Fig. 6(e), shows that the addition of noise makes $P_E(\Delta f)$ increase approximately 1.23 times for every Δf. The ratio for the product of P_E and P_R, as the denominator of C_{ER}, can be obtained by simply shifting the ratio of P_R (red

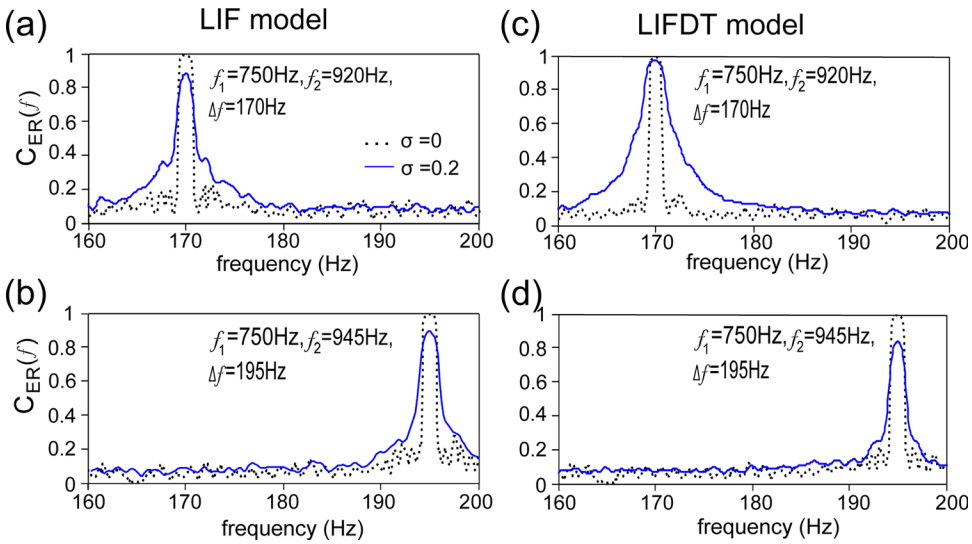

FIG. 5. (Color online) Coherence function between $E(t)$ and $R(t)$, denoted by C_{ER}, obtained from (a) and (b) LIF model or (c) and (d) LIFDT model, shows a peak at the beat frequency Δf. When σ increases from zero (dashed black lines) to 0.2 (solid blue lines), $C_{ER}(\Delta f)$ in (a) and (b) decreases when $\Delta f = 170$ or 195 Hz. For the LIFDT model, upon increasing σ, $C_{ER}(\Delta f)$ decreases when $\Delta f = 195$ Hz in (d) but remains near 1 with $\Delta f = 170$ Hz in (c). Fifty independent realizations of η and ξ in I_{stim} were used to average the coherence when $\sigma > 0$ and same in following figures.

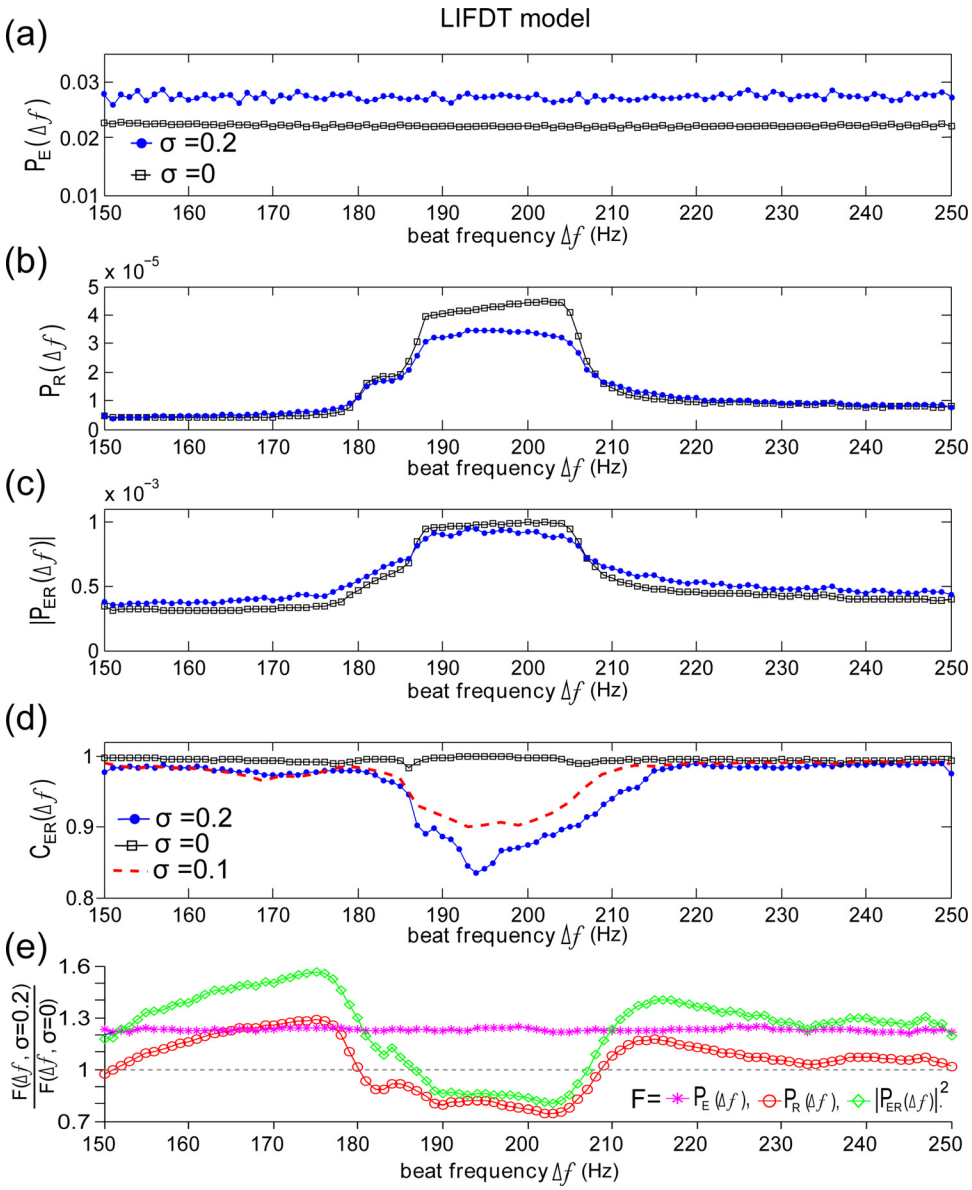

FIG. 6. (Color online) (a) $P_E(\Delta f)$, (b) $P_R(\Delta f)$, (c) the magnitude of cross-spectral density between envelope and spike train, $|P_{ER}(\Delta f)|$, and (d) $C_{ER}(\Delta f)$ calculated from the LIFDT model were plotted as functions of Δf with $\sigma = 0$ (black squares) or $\sigma = 0.2$ (blue dots). The ratio of $F(\Delta f, \sigma = 0.2)$ (the values of a function F calculated with $\sigma\eta$) to $F(\Delta f, \sigma = 0)$ (the function values obtained in the absence of $\sigma\eta$) was plotted in (e). Because of the resonance, $P_R(\Delta f)$ in (b) shows a bump over [185, 208] Hz where $\Delta f \approx f_m$; $\sigma\eta(t)$ leads to a coherence depression in (d). A larger σ further suppresses $C_{ER}(\Delta f)$.

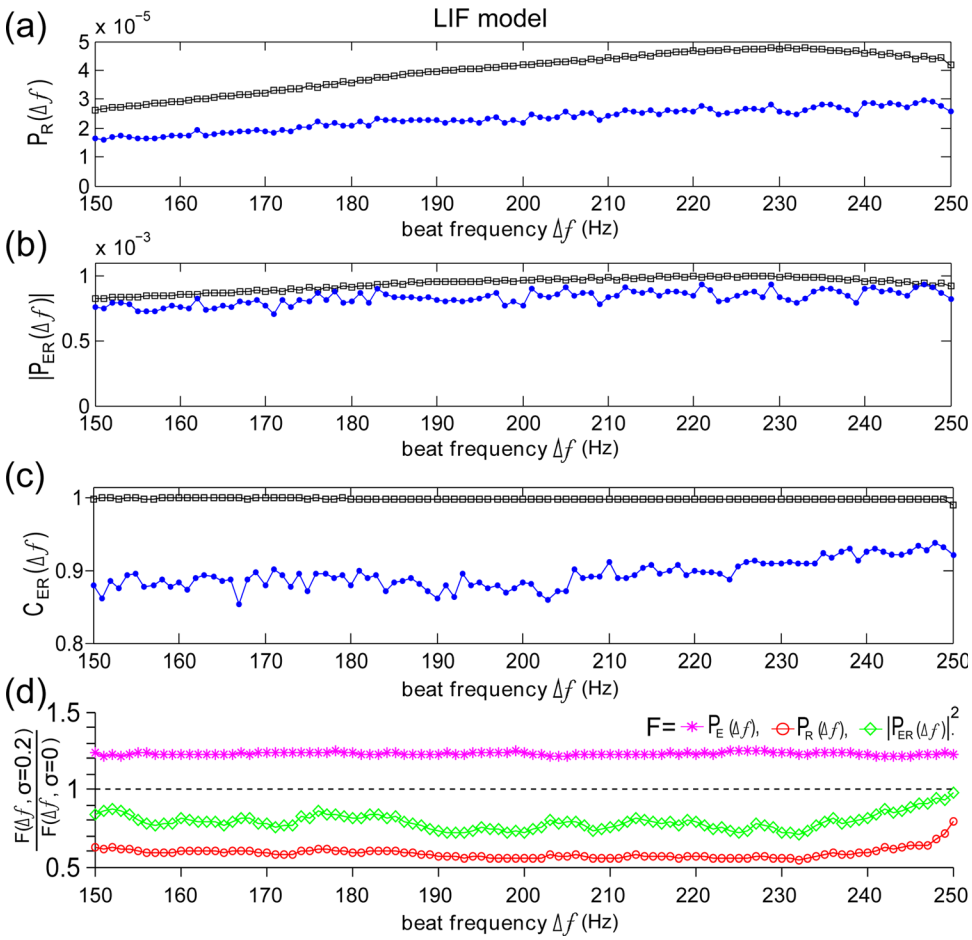

FIG. 7. (Color online) (a) $P_R(\Delta f)$, (b) $|P_{ER}(\Delta f)|$, and (c) $C_{ER}(\Delta f)$ calculated from the LIF model were plotted as functions of Δf with $\sigma = 0$ (black squares) or $\sigma = 0.2$ (blue dots). The ratio of $F(\Delta f,\sigma = 0.2)$ to $F(\Delta f,\sigma = 0)$ was plotted in (d). Here, the envelope noise causes coherence depression all over the test frequency range.

circles) vertically to 1.23 times higher. Thus, the shifted P_R ratio matches with the ratio of $|P_{ER}|^2$ (green diamonds) well outside of the sensitive regime, but the former is higher than the latter within the sensitive regime. Given that $C_ER(\Delta f) \approx 1$ with $\sigma = 0$, we could estimate $C_{ER(\Delta f)} < 1$ over approximately [185, 208] Hz and $C_{ER(\Delta f)} \approx 1$ elsewhere. This coherence reduction is caused by the further decrease of P_{ER} under the influence of envelope noise.

$C_{ER}(\Delta f)$ obtained from the LIF model is suppressed by AM noise all over the test frequency range, as Fig. 7 shows, based on the same reasoning. The comparison between the LIFDT and LIF models implies that the dynamic threshold enhances the correlation between envelope and spike train, with or without envelope noise, when Δf is away from the intrinsic frequency, thus improves the linear encoding of stimuli. However, when the beat frequency is close to the intrinsic frequency of the LIFDT model, the resonance along with AM noise significantly increases both envelope fluctuations and ISI variability, and consequently reduces the correlation between $E(t)$ and $R(t)$ and eventually suppresses C_{ER}.

With increased σ values from 0 to 0.2, Fig. 5(d) displays that coherence is further suppressed by larger intensity of AM noise. We next focused on C_{ER} with fixed $\Delta f = 195$ Hz and examine the influences of A_2 and σ on it. Figure 8 demonstrates that A_2 enhances $C_{ER}(\Delta f = 195)$; however, increasing σ causes a stronger coherence depression. This also indicates that the ratio of σ/A_2, reflecting the CV of the envelope, is positively correlated with the degree of coherence depression.

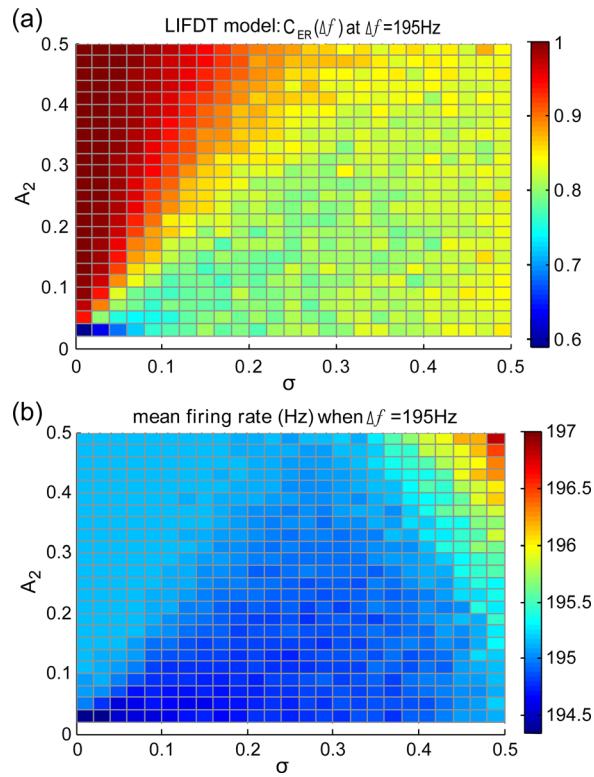

FIG. 8. (Color online) When Δf is fixed at 195 Hz, (a) $C_{ER}(\Delta f)$ obtained from the LIFDT model increases with A_2 but decreases with σ and (b) the corresponding meaning firing rate changes slightly. The bar on the right shows color codes corresponding to the value of $C_{ER}(\Delta f)$ (a) or mean firing rate (b), respectively.

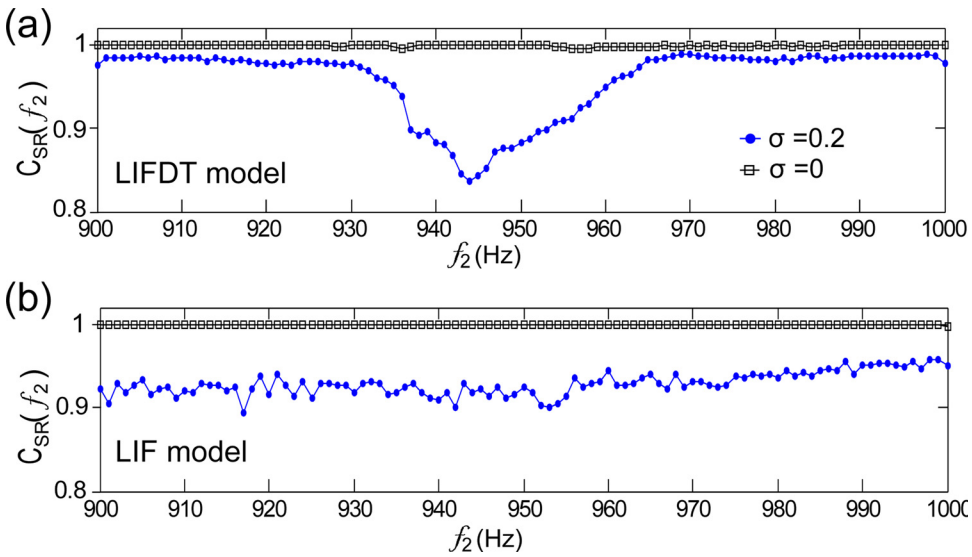

FIG. 9. (Color online) Coherence function between the stimulus signal I_{stim} and spike train $R(t)$, C_{SR}, as a function of f_2 for (a) the LIFDT model and (b) the LIF model.

D. Depression of Stimulus-Response Coherence

We also calculated the coherence function between I_{stim} (rather than just its envelope) and $R(t)$, denoted as C_{SR}, as a function of f_2 for both models. Figure 9 demonstrates that $\sigma\eta$ reduces $C_{SR}(f_2)$ everywhere, but particularly between about 935 Hz to 958 Hz, corresponding to the sensitive regime where C_{ER} depression happens. Also, this noise suppresses $C_{SR}(f_2)$ of the LIF model everywhere. We note that Figs. 4(a) and 4(b) showed that non-zero σ decreased $P_R(\Delta f)$ and $P_R(f_2 = f_1 + \Delta f)$ of the LIFDT model simultaneously when $\Delta f \approx f_m$. The same reason that we stated previously for C_{ER} depression can be used to explain C_{SR} reduction as well.

E. Coherence depression driven by SAM

In order to further assess the generality of coherence depression, we also used a SAM of a carrier, which involves a product of two sinusoids, instead of the sum of two sinusoids as used up to now. Such SAM stimuli have been used widely in particular in electrosensory systems research. Here, we used more specifically a SAM with a stochastic amplitude, which leads to the following form of the stimulus:

$$I_{SAMstim} = [A_1 + (A_2 + \sigma\eta(t))\sin(2\pi f_{SAM} t)]\sin(2\pi f_1 t) + I + \epsilon\xi(t). \quad (10)$$

Here the frequency of the SAM, f_{SAM}, is regarded as the beat frequency, Δf. Other parameters take the corresponding values as in Eq. (1). The simulation results, as demonstrated in Fig. 10, of the LIFDT model with Eq. (10) as the stimulus shows a similar coherence depression pattern as with the original signal in Eq. (1).

IV. DISCUSSION AND CONCLUSION

We have performed a comparison between the responses of LIFDT and LIF models to a sum of two incommensurate sine waves with an AM noise included in the envelope of the second wave. Those frequencies as well as the associated beat frequency are expressed in the spike trains of the neuron models. Using numerical simulations, we have demonstrated that the existence of the dynamic firing threshold in the LIFDT model causes a decreased slope of the F-I curve as well as different resonance properties and susceptibilities to AM noise.

We then showed how different spectral properties for the fixed and the dynamic firing threshold models lead to qualitatively different patterns of envelop—spike train coherence in the presence of AM noise. For the classical LIF model with constant firing threshold, a coherence depression over the whole frequency domain was found. Such a drop in input-output coherence due to noise is to be expected. However, interestingly, for the LIFDT model in which the firing

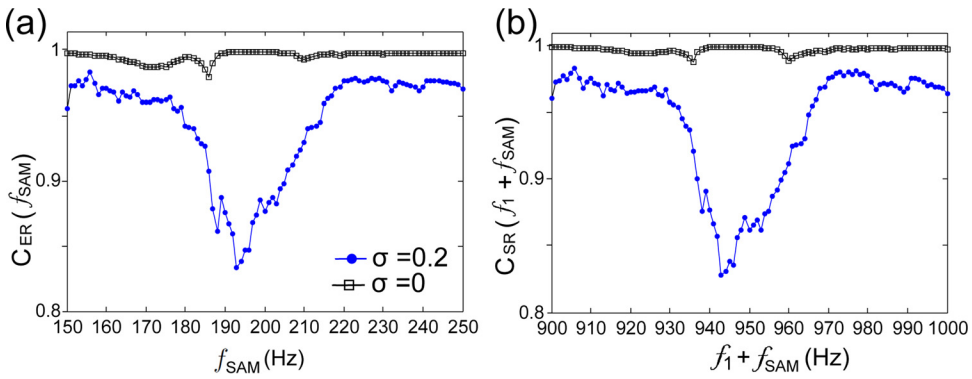

FIG. 10. (Color online) When $I_{SAMstim}$ (10) with SAM is used as input to the LIFDT model, $C_{ER}(f_{SAM})$ and $C_{SR}(f_1 + f_{SAM})$ display depression.

threshold is dynamic and perpetuates memory of past spiking events, the coherence depression happens only in the proximity of the intrinsic frequency of the model; outside this range the model displays a high coherence near one. Our simulation also demonstrates that coherence function has similar pattern when a periodic stimulus at the frequency equal to the mean firing rate and containing a slow noise in its amplitude is applied (not shown.)

The firing mechanism of the LIFDT model is more elaborate than that of classic LIF model. The former is controlled by three factors: the spike-driven dynamic firing threshold, driving force (in particular its envelope in our case) and AM noise expressed in envelope. This dynamic threshold works like a band-pass filter,[42] which enhances frequencies within a limited range centred on the intrinsic firing rate. Outside that range, the dynamic threshold filters out the slow AM noise—which is in a lower frequency range than the beat frequency), and consequently sustains the envelope—spike train coherence.

However within that range, the resonance-induced synchrony between envelope and spike trains dominates. AM noise causes both envelope fluctuations and high variability of ISIs, which leads to a low correlation between envelope and spike trains. And this eventually results in a reduction of coherence function. On the other hand, frequency synchrony could be an efficient mechanism for signal transmission, depending on the post-synaptic mechanism to read out the information, but our results show that its performance would be impaired by noise. This implies that the dynamic threshold might be a strategy to compensate the transmission deficit induced by noise, at least outside the range of the intrinsic firing frequency.

The dynamic firing threshold is also a simple mechanism to mimic the refractory properties of neurons. There is in fact no need to include an absolute refractory property in that model, since the dynamic threshold prevents unrealistically short ISIs. Its nonlinear property of envelope transmission makes the separation of spectral peaks at frequencies corresponding to the envelope frequency and intrinsic firing rate very difficult except in the case of resonance. More realistic excitable systems such as the Morris-Lecar model or Hodgkin-Huxley models intrinsically possess a refractory period due to the action potential width. Further, real neurons can exhibit firing threshold fluctuations as in the LIFDT model which is well modeled by temporary shifts in the activation curves.[43] Hence, these models could have similar coherence depression in a certain condition, for example when the driving frequency is close to their intrinsic firing frequencies.

We note that the LIFDT model belongs to the class of adaptive neuron models, because the threshold evolves as a function of past history. Following a spike, increasing the threshold or adding a negative current—as an ionic adaptation current would—leads to similar dynamics overall, although there are some distinctions.[40] While we have not investigated this possibility here, it is likely that a leaky integrate-and-fire type model with adaptation current—would exhibit the coherence depression effect revealed in our study. This is also expected for Hodgkin-Huxley models with dynamic threshold or adaptive current.

Finally, in the context of electrosensation, our findings suggest that P-unit electroreceptors would show less coherence to a beat if the beat frequency is close to the mean firing rate of the P-unit. Different receptors have different intrinsic firing rates with a distribution well-fitted to a log-normal distribution.[44] The precise origin and usefulness of this distribution are unknown. Combined with the distribution of carrier frequencies of different fish in the same species - not to mention other species - which sets the intrinsic firing rate of the receptors, this implies that typical beats caused by the presence of other fish could often fall near the intrinsic rate of specific receptors. The ensuing reduction in coherence, uncovered in our paper, and possible loss of information, may have implications for this distribution and perhaps even for the need to shift the carrier frequencies of the fish to accommodate their array of receptors.

ACKNOWLEDGMENTS

This work was supported by the Natural Sciences and Engineering Research Council of Canada (NSERC). AL has fond memories of working with Frank Moss, to which this article and special issue are dedicated, and is very grateful for the mentoring he provided.

APPENDIX: SPECTRAL ANALYSIS OF THE ENVELOPE AND SPIKE TRAIN

We take the SAM signal $(A_2+\sigma\eta\ (t))\sin(2\pi\Delta ft)$, as an example to analytically show how AM noise $\sigma\eta(t)$ increases the value of $P_E(\Delta f)$. Here the effect of white noise on the envelope is ignored as its intensity is very low compared with that of the AM noise. The Fourier transform (FT) of the OU process $\eta(t)$ can be easily derived from its differential equation:

$$\mathcal{F}[\eta(t)] = \frac{\sqrt{2\gamma}}{\gamma + i2\pi f}. \tag{A1}$$

Thus, FT of the SAM can also be calculated:

$$\begin{aligned}\mathcal{F}[E(t)] &= A_2\mathcal{F}[\sin(2\pi\Delta ft)] + \sigma\mathcal{F}[\eta(t)] * \mathcal{F}[\sin(2\pi\Delta ft)] \\ &= -iA_2\delta(f-\Delta f) + \frac{\sigma\sqrt{2\gamma}}{[i\gamma - 2\pi(f-\Delta f)]}\end{aligned} \tag{A2}$$

where * denotes the convolution operation. Thus, the power spectral density of the SAM can be obtained as

$$P_E(f) = A_2^2\delta(f-\Delta f) + \frac{2\gamma[\sigma^2 + A_2\delta(f-\Delta f)]}{\gamma^2 + 4\pi^2(f-\Delta f)^2}. \tag{A3}$$

Thus, Eq. (13) clearly shows that $P_E(f)$ has a peak at Δf. The second term in Eq. (A3) is the positive contribution of AM noise that increases the value of $P_E(\Delta f)$. Larger σ broadens the width of this peak and increases the noise floor.

In order to understand the mechanism why AM noise decreases the height of $P_R(\Delta f)$ shown in Fig. 4, we can also estimate $P_R(f)$ for the LIF model and for the LIFDT model when Δf is in the vicinity of intrinsic frequency. For simplicity,

we can approximate the spike times as a periodic component plus a random uncorrelated component τ_k, as in Ref. 45: $t_k = k/\Delta f + \tau_k$. The periodic component arises because upstrokes of the envelope and spike events are nearly in a 1:1 correspondence. τ_k is a set of random variables and arise from the sources of noise in the dynamics, namely, the AM noise η and the additive noise ξ. τ_k is assumed independent of τ_l for any $l \neq k$ and they are assumed to share same mean zero and same probability density function $\phi(\tau)$. The approximation of power spectra of such constant frequency spike train with jitter has be given by[45]

$$P_R(f) = \Delta f[1 - |\Phi(f)|^2 + \Delta f|\Phi(f)|^2 \sum_k \delta(f - k\Delta f)] \quad \text{(A4)}$$

where $\Phi(f)$ is the Fourier transform of probability density function $\phi(\tau)$. The first two terms of Eq. (A4) are continuous and produce the noise floor of the power spectra of spike trains. The last term, demonstrated as discrete spectral peaks as shown in Fig. 4 and weighted by $|\Phi(f)|^2$, reflects the underlying periodicity of spike train. For simplicity, τ_k follows a Gaussian distribution with mean zero and standard deviation σ_τ. By substituting the Fourier transform of its probability density function, $\Phi(f) = \exp(-2\pi\sigma_\tau^2 f^2)$, into Eq. (A4), we have

$$P_R(f) = \Delta f[1 - e^{-4\pi\sigma_\tau^2 f^2} + \Delta f e^{-4\pi\sigma_\tau^2 f^2} \sum_k \delta(f - k\Delta f)]. \quad \text{(A5)}$$

The spectral peaks have equal height in the absence of noise (i.e., $\sigma_\tau = 0$). However, with noise, the highest peak is located at Δf, since $\exp(-4\pi\sigma_\tau^2 f^2)$ decays with f. This height decreases with increasing σ_τ (or equivalently with increasing σ in the AM noise).

[1] B. Lindner, J. Garcia-Ojalvo, A. Neiman, and L. Schimansky-Geier, Phys. Rep. **392**, 321 (2004).
[2] F. Moss, L.W. Ward, and W.G. Sannita, Clin. Neurophysiol. **115**, 267 (2004).
[3] R. Benzi, G. Parisi, A. Sutera, and A. Vulpiani, Tellus **34**, 10 (1982).
[4] J. J. Collins, C. C. Chow, and T. T. Imhoff, Phys. Rev. E **52**, 3321 (1995).
[5] K. Park, Y.-C. Lai, Z.-H. Liu, and A. Nachman, Phys. Lett. A **326**, 391 (2004).
[6] N. G. Stocks, Phys. Rev. Lett. **84**, 2310 (2000).
[7] M. D. McDonnell, N. G. Stocks, C. E. M. Pearce, and D. Abbott, Phys. Lett. A **352**, 183 (2006).
[8] A. B. Neiman and D. F. Russell, Phys. Rev. Lett. **88**, 138103 (2002).
[9] D. R. Chialvo, Chaos, **13**, 1226 (2003); O. Calvo and D. R. Chialvo, Int. J. Bifurcat. Chaos Appl. Sci. Eng. **16**, 731 (2006).
[10] P. J. Thomas, P. H. E. Tiesinga, J.-M. Fellous, and T. J. Sejnowski, Neurocomputing **52–54**, 955 (2003).
[11] P. H. E. Tiesinga, Phy. Rev. E **65**, 041913 (2002).
[12] D. D. Greenwood, J. Acoust. Soc. Am. **79**, 1857 (1986).
[13] I. A. Khovanov and P. V. E. McClintock, Phys. Rev. E **76**, 031122 (2007).
[14] W. Heiligenberg, *Neural Nets in Electric Fish* (Cambridge, MA, 1991).
[15] M. Chacron, A. Longtin, M. St-Hilaire, and L. Maler, Phys. Rev. Lett. **85**, 1576 (2000).
[16] H. v. Helmholtz, *On the Sensations of Tone as a Physiological basis of the Theory of Music* (F. Vieweg und sohn, Braunschweig, 1863), translated by Alexander Ellis (Dover Publications, New York, 1954).
[17] P. X. Joris, C. E. Schreiner, and A. Rees, Physiol. Rev. **84**, 541 (2004).
[18] A. Neiman, L. Schimansky-Geier, and F. Moss, Phys. Rev. E **56**, R9 (1997).
[19] H. L. Van Tress, *Detection, Estimation, and Modulation Theory: Part III, Radar-Sonar Signal Processing and Gaussian Signals in Noise* (Wiley, New York, 1971).
[20] O. Besson, P. Stoica, and A. B. Gershman, IEEE Trans. Signal Process **49**, 730 (2001).
[21] Z. M. Smith, B. Delgutte, and A. J. Oxenham, Nature (London) **416**, 87 (2002).
[22] C. J. Condon, K. R. White, and A. S. Feng, J. Comp. Physiol., A **178**, 147 (1996).
[23] S. Wohlgemuth, A. Vogel, and B. Ronacher1, J. Comp. Physiol. **197**, 61 (2011).
[24] J. W. Middleton, A. Longtin, J. Benda, and L. Maler, Proc. Natl. Acad. Sci. U.S.A. **23**, 14596 (2006).
[25] W. S. Geisler, D. G. Albrecht, and A. M. Crane, J. Neurosci. **27**, 5063 (2007).
[26] H. Tanaka and I. Ohzawa, J. Neurosci. **26**, 4370 (2006).
[27] P. V. McGraw, D. M. Levi, and D. Whitaker, Nat. Neurosci. **2**, 479 (1999).
[28] Y. H. Liu and X.-J. Wang, J. Comput. Neurosci. **10**, 25 (2001).
[29] N. G. Stocks, D. Abbott, and R. P. Morse, Proc. SPIE **5841**, 23 (2005).
[30] A.-S. Pan, Y. Zhang, and P. A. Parker, Med. Biol. Eng. Comput. **27**, 14 (1989).
[31] C. Gómez, J. M. Quero, and M. Escudero, Int. J. Bio-Med. Comput. **24**, 207 (1989).
[32] R. Maex and E. De Schutter, J. Neurosci. **23**, 10503 (2003), http://www.jneurosci.org/content/23/33/10503.short.
[33] D. R. Bach, J. G. Neuhoff, W. Perrig, and E. Seifritz, Int. J. Psychophysiol. **74**, 28 (2009).
[34] B. Boashash, Proc. IEEE **80**, 520 (1992).
[35] F. Gabbiani, Network **7**, 61 (1996).
[36] A. Borst and F. Theunissen, Nat. Neurosci. **2**, 947 (1999).
[37] J. W. Middleton, E. Harvey-Girard, L. Maler, and A. Longtin, Phys. Rev. E **75**, 021918 (2007).
[38] S. Hong, B. N. Lundstrom, and A. L. Fairhall, PLOS Comput. Biol. **4**, e1000119 (2008).
[39] C. Sutherland, B. Doiron, and A. Longtin, Biol. Cybern. **100**, 475 (2009).
[40] J. Benda, L. Maler, and A. Longtin, J. Neurophysiol. **104**, 2806 (2010).
[41] B. Lindner and L. Schimansky-Geier, Phys. Rev. Lett. **86**, 2934 (2001).
[42] J. Benda, A. Longtin, and L. Maler, J. Neurosci. **25**, 2312 (2005).
[43] M. J. Chacron, B. Lindner, and A. Longtin, J. Comp. Neurosci. **23**, 301 (2007).
[44] D. Gussin, J. Benda, and L. Maler, J. Neurophysiol. **97**, 2917 (2007).
[45] J. C. Coggshall, Kybernetik **13**, 30 (1973).